Published in final edited form as:
J Am Chem Soc. 2010 August 11; 132(31): 10842–10846. doi:10.1021/ja102758v.

Rational Design and Simple Chemistry Yield a Superior, Neuroprotective HDAC6 Inhibitor, Tubastatin A

Kyle V Butler[1], **Jay Kalin**[1], **Camille Brochier**[2], **Guilio Vistoli**[3], **Brett Langley**[2], and **Alan P Kozikowski**[1,*]

[1]Drug Discovery Program, Department of Medicinal Chemistry and Pharmacognosy, University of Illinois at Chicago, 833 South Wood, Chicago, Illinois, 60612, USA, and, Chicago, Illinois 60612

[2]Burke Medical Research Institute, 785 Mamaroneck Avenue, White Plains, NY 10605, USA

[3]Dipartimento di Scienze Farmaceutiche “Pietro Pratesi”, Università degli Studi di Milano, Via Mangiagalli 25, I-20133 Milan, Italy

Abstract

Structure-based drug design combined with homology modeling techniques were used to develop potent inhibitors of HDAC6 that display superior selectivity for the HDAC6 isozyme compared to other inhibitors. These inhibitors can be assembled in a few synthetic steps, as thus are readily scaled up for *in vivo* studies. An optimized compound from this series, designated Tubastatin A, was tested in primary cortical neuron cultures in which it was found to induce elevated levels of acetylated α-tubulin, but not histone, consistent with its HDAC6 selectivity. Tubastatin A also conferred dose-dependent protection in primary cortical neuron cultures against glutathione depletion-induced oxidative stress. Importantly, when given alone at all concentrations tested, this hydroxamate-containing HDAC6-selective compound displayed no neuronal toxicity, thus forecasting the potential application of this agent and its analogs to neurodegenerative conditions.

Introduction

Protein function can be regulated by the enzymatic addition and removal of acetyl groups at specific lysine residues. Lysine acetylation is mediated by two classes of enzymes with opposing functions: histone acetyltransferase (HAT) and histone deacetylase (HDAC), which catalyze the addition and removal of acetyl groups, respectively.1 The domain of this regulatory mechanism is vast: mass spectrometry profiling identified 3600 sites on 1750 proteins subject to acetylation.2 HDAC inhibitors (HDACI) have been aggressively pursued as therapies for cancer and CNS disorders, and two inhibitors, Vorinostat and Romidepsin, have been FDA approved for treatment of cutaneous T-cell lymphoma.3 HDACIs act on eleven zinc-dependent HDAC isozymes; their classification and properties have been reviewed elsewhere.4,5 These enzymes are divided into four groups: class I (HDACs 1, 2, 3, 8), class IIa (HDACs 4, 5, 7, 9), class IIb (HDACs 6, 10), and class IV (HDAC11). Most HDACI so far identified primarily inhibit the class I enzymes, producing an antiproliferative phenotype which is useful for oncology applications, but unwarranted for the many non-oncology applications of these agents.6 The potential toxicities associated with the inhibition of certain isozymes may lead to additional difficulties for the clinical development

kozikowa@uic.edu.

Supporting Information Available: Experimental details for synthesis of all compounds shown, synthesis of additional compounds and their enzyme inhibition data, structures of referenced compounds, procedures for enzyme inhibition assays, additional homology modeling figures, TSA neuroprotection data, and western blot analysis procedures are included in the supporting information section. This material is available free of charge via the Internet at http://pubs.acs.org.

of pan-HDAC inhibitors.7–9 Because the network of cellular effects mediated by acetylation is so vast and because inhibition of some isozymes may lead to undesirable side effects, isozyme selective inhibitors may hold greater therapeutic promise than their nonselective counterparts.10

HDAC6 has emerged as an attractive target for drug development and research.11,12 A diverse set of substrates have been identified for this enzyme, including α-tubulin, HSP90, peroxiredoxins, and nuclear histones.13–15 Presently, HDAC6 inhibition is believed to offer potential therapies for autoimmunity, cancer, and many neurodegenerative conditions.9,16–18 Selective inhibition of HDAC6 by small molecule or genetic tools has been demonstrated to promote survival and re-growth of neurons following injury, offering the possibility for pharmacological intervention in both CNS injury and neurodegenerative conditions.19 Unlike other histone deacetylases, inhibition of HDAC6 does not appear to be associated with any toxicity, making it an excellent drug target.7 Tubacin, an HDAC6 selective inhibitor, was identified in 2003 by combinatorial chemistry methods.20 The use of Tubacin in models of disease has helped to validate, in part, HDAC6 as a drug target, but its non-drug-like structure, high lipophilicity (ClogP = 6.36 (KOWWIN)), and tedious synthesis conspire to make it more useful as a research tool than a drug.21 Other compounds have been reported to have modest preference for HDAC6.22–24 Encouraged by the possible use of HDAC6 inhibitors as neuroprotective agents, we initiated a drug design campaign to identify highly selective and drug-like inhibitors of this enzyme. We now show how rational drug design was used to generate an HDAC6 inhibitor with a drug-like structure, simple synthesis, and superior target selectivity.

Results and Discussion

Homology Modeling

We chose to study selectivity by comparing HDAC6 against HDAC1, the latter being an important regulator of cell proliferation and a key oncology target. Their comparison is most useful, as these two enzymes have diverse phylogeny and are members of separate deacetylase classes. Lacking crystal structures for both subtypes, we generated reliable models for these isozymes by employing homology techniques.

HDAC1 and HDAC6 homology models were generated by exploiting multiple resolved HDAC crystal structures as templates, followed by multiple-threading alignments, as implemented in the I-TASSER approach.25 I-TASSER is an automated bioinformatics tool for predicting protein structure from amino acid sequence. The catalytic sites of both models were established by extracting zinc and chelating residues from the human HDAC8 structure in complex with trichostatin A (PDB: 3FOR) and inserting them into the generated models. Analysis of the two modeled catalytic pockets revealed that while the active site is highly conserved, the dimensions of the catalytic channel rim differ greatly between the two isozymes. Figure 1 shows four regions, A–D, which represent boundaries of the catalytic channel rim. Region A corresponds to P32 in HDAC1 and P501 in HDAC6; region B corresponds to L271 and Y204 in HDAC1 and L749 and F679 in HDAC6; region C corresponds to D99 and F205 in HDAC1 and D567 and F680 in HDAC6; region D corresponds to Q26, G27, M30, and K31 in HDAC1 and S498, H500, E502, and V503 in HDAC6. Variation at the D region produces a significantly wider channel rim in the homology model of HDAC6. The structural manifestation of this variation is that the measured D-B distance in the energy minimized conformation is 12.5 Å in HDAC1, compared to 17.5 Å in HDAC6. Following the canonical HDACI structure of aromatic cap group – linker – hydroxamic acid, we sought to design compounds that target this area of structural diversity with a cap group that is both large and rigid enough to comfortably occupy the rim region of HDAC6, but not HDAC1. After investigating various polycyclic

cap group frameworks, the carbazole system was found to fit these criteria. When attached to a zinc-chelating hydroxamic acid by an appropriate linker, the carbazole nicely fits the D region of HDAC6, whereas it clashes with the B and D regions in HDAC1 (Figure 3, supporting information).

Design of tricyclic HDACI and enzyme inhibition data

While lined with conserved residues, the modeled catalytic channels of HDAC1 and HDAC6 also differ in shape. The HDAC6 channel appears wider and shallower; suggesting that replacement of the traditional alkyl chain linker with bulkier and shorter aromatic moieties might further enhance HDAC6 selectivity. A series of carbazole hydroxamic acids with alkyl and alkylaryl linker groups were synthesized (supporting information). Inhibitor selectivity was monitored by comparing IC_{50} values at HDAC6 against HDAC1 by assays using purified human HDAC protein. All of the carbazole-based compounds preferentially inhibited HDAC6. (Table 1). Ease of synthesis was of paramount importance to our drug design, and most of these inhibitors can be made in two or three steps. The simple syntheses allowed for rapid generation of structural analogs. For carbazoles with alkyl chain linkers, the *n*-pentyl linker (**1**) was best, giving good potency with approximately 226-fold selectivity. The optimal linker was the *p*-tolyl group of **5**, which had an IC_{50} value of 19 nM at HDAC6 with approximately 574 fold selectivity over HDAC1. For **5**, the angle between the rotational axis of the tolyl linker and the $C(sp^3)$-N bond connecting linker and cap is fixed at ~113°, forcing the carbazole to lay against the catalytic channel rim, stressing the reported differences between the two rim regions.

We next examined how modifications to the tricyclic group influenced activity. As the carbazoles are too lipophilic to be good drugs, we reduced lipophilicity by disrupting planarity in the tricyclic ring system and introducing a tertiary amine. Analogs of **1** (compounds **2**–**4**) were less potent than the parent, but all preferentially inhibited HDAC6. Analogs of **5** displayed enhanced potency and selectivity. The tetrahydro-γ-carboline analog, **6**, was superior to the parent in HDAC6 potency and selectivity, with an IC_{50} of 15 nM at HDAC6 and over 1000-fold selectivity against HDAC1. The tetrahydro-β-carboline, **7**, was even better, with an IC_{50} of 1.4 nM at HDAC6 and approximately 3700-fold selectivity against HDAC1. We note that modifications to the tricyclic group did not significantly enhance inhibitory activity when employed in conjunction with the *n*-pentyl linker, but greatly enhanced activity and selectivity when used with the tolyl linker, where the bent conformation forces tighter interactions between the tricycle and the catalytic channel rim, giving a greater response to structural changes made to the tricycle. The enhanced selectivity of the carboline derivatives may also derive from the presence of the N-methyl group, as this substituent will further expand the dimensions of the cap group, further favoring interactions with HDAC6.

The tricyclic inhibitors were compared with other compounds reported to be highly selective for HDAC6. Tubacin was found to potently inhibit HDAC6, with an IC_{50} value of 4 nM and approximately 350-fold selectivity over HDAC1. The optimized inhibitors, **6** and **7**, are far more selective for HDAC6 than any other compounds reported in literature. These agents are also very druggable: ClogP = 2.41 (KOWWIN) and tPSA = 57 for both **6** and **7**; AlogPs water solubility = 45.2 mg/l for **6** and 43.7 mg/l for **7**. The tertiary amine group can be used to form pharmaceutically useful salts, thus facilitating compound solubilization. Furthermore, their facile, three-step syntheses allow easy scale-up for *in vivo* studies. These compounds confirm our structure based design approach, as less than 30 compounds were made to arrive at these findings.

To further validate this compound series, we chose to profile HDACI **6**, hereafter designated as Tubastatin A, against all 11 isozymes, to investigate its ability to induce α-tubulin

acetylation in cells, as well as to profile its neuroprotective action in a cell model of oxidative stress. This compound was chosen for further profiling after it was found to have favorable *in vitro* ADME properties. Thus, both Tubastatin A and Tubacin were tested at all 11 HDAC isoforms. (Table 2) Tubastatin A was substantially more selective than Tubacin at all isozymes except HDAC8 and maintained over 1000-fold selectivity against all isoforms excluding HDAC8, where it had approximately 57-fold selectivity. The moderate activity of Tubastatin A at HDAC8 may be the product of a known conformational change that occurs upon binding to HDAC8, which dilates the catalytic pocket, to better accommodate the bulky tricyclic group.27

Selectivity of Tubastatin A was analyzed in the more complex cellular environment by comparing α-tubulin hyperacetylation, corresponding to HDAC6 inhibition, with histone hyperacetylation, which corresponds to class I HDAC inhibition. (Figure 2) Both Tubastatin A and Tubacin preferentially induced α-tubulin hyperacetylation at 2.5 μM. Slight induction of histone hyperacetylation was seen for Tubastatin A at 10 μM, which may reflect inhibition of the limited histone deacetylase activity of HDAC6 or slight inhibition of class I HDACs at these higher concentrations.

Analysis of Tubastatin A in a model of neurodegeneration

Previously, it has been shown that inhibition of HDAC6 protects against neuronal degeneration and stimulates neurite outgrowth in dorsal root ganglion neurons, thus suggesting a means for achieving therapeutic intervention in CNS diseases.19 Tubastatin A was examined in a model of oxidative stress induced by homocysteic acid (HCA). This model leads to depletion of glutathione, the cells major intracellular antioxidant. HDAC6 inhibition rescues neuronal death in this model, possibly by causing hyperacetylation of peroxiredoxins. In previous work, we reported that nonselective, hydroxamic acid HDACIs displayed considerable toxicity to the primary cortical neurons.28 In HCA-induced neurodegeneration assays, TSA was moderately neuroprotective at 0.5 μM, although protection declined at higher concentrations due to dose-dependant neurotoxicity. Tubastatin A displayed dose-dependent protection against HCA-induced neuronal cell death starting at 5 μM with near complete protection at 10 μM. (Figure 3) This result compares well with results reported by Parmigiani et al., showing that Tubacin induces α-tubulin acetylation at 5 μM and protects prostate cancer (LNCaP) cells from hydrogen peroxide-induced death at 8 μM via peroxiredoxin acetylation.29 Importantly, when tested alone at all of the concentrations shown, Tubastatin A exhibited no toxicity, indicating that neurotoxicity is likely a product of class I HDAC inhibition, and not a property inherent to hydroxamic acids. Tubastatin A is the first neuroprotective hydroxamic acid-based HDACI that we have found, that does not cause neuronal death when tested alone in the HCA model. These results provide further evidence that the inhibition of HDAC6 may provide a means for achieving therapeutic intervention in neurodegenerative conditions.

In summation, this work presents compounds that exhibit outstanding selectivity and potency for the inhibition of HDAC6. Rational drug design principles combined with homology modeling have made it possible to create these novel chemical entities which can be assembled in multi-gram quantities in a few days time. The *in vitro* enzyme biology is consistent with cellular activity, and multiple *in vivo* studies, which will be the subject of future reports, demonstrate the superior biological profile of Tubastatin A in various models of inflammation.

Experimental Details

Homology and molecular modeling

Human HDAC sequences were obtained from the UniProt database (www.uniprot.org). Multiple sequence alignments of HDAC isozymes were carried out using CLUSTALW and BLOSUM matrices for alignment scoring (www.clustal.org). The HDAC1 and HDAC6 homology models were generated by exploiting resolved crystal structures as templates, followed by multiple-threading alignments, as implemented in the I-TASSER approach (zhang.bioinformatics.ku.edu/I-TASSER). For HDAC6, modeling focused on the sole second catalytic subunit (CDII, Gly482-Gly801), as it is the major functional domain of HDAC6. Following construction of the models, hydrogen atoms were added using VEGA (www.vegazz.net). To remain compatible with physiological pH values, the side-chains of Arg, Lys, Glu, and Asp were ionized, while His and Cys residues were considered neutral by default. The complete models were carefully checked to avoid unphysical occurrences such as cis peptide bonds, wrong configurations or colliding side-chains. A preliminary energy minimization was performed on the models to avoid high-energy interactions, in which the backbone atoms were fixed to preserve the predicted folding.

In order to correctly arrange zinc at the catalytic site, metal ion and chelating residues were extracted from the resolved structure of human HDAC8 complexed with trichostatin A (PDB: 3FOR) and inserted into the generated models. This was accomplished by superimposing the C_α carbon atoms of the zinc-coordinating residues in PDB:3FOR over the corresponding atoms of HDAC1 and HDAC6. All atoms except the zinc ion were then deleted. Finally, an energy minimization was performed by fixing the backbone and zinc ion, completing the homology modeling procedure.

The optimized models were exploited for docking simulations. The conformational behavior of simulated compounds was investigated by a MonteCarlo procedure (as implemented in the VEGA suite of programs which generated 1000 conformers by randomly rotating the rotors). All geometries obtained were stored and optimized to avoid high-energy rotamers. The 1000 conformers were clustered by similarity to discard redundancies; in this analysis, two geometries were considered non-redundant when they differed by more than 60 degrees in at least one torsion angle. For each derivative, the lowest energy structure was then submitted to docking simulations. All minimizations were carried out on a 16 CPU Tyan-VX50 system using Namd2.6 with CHARMM force field and Gasteiger's atomic charges.

Docking calculations were carried out on the HDAC1 and HDAC6 models by AutoDock4.0. The grid boxes were set to include all residues within a 15 Å radius sphere around the catalytic Zn ions thus comprising the entire catalytic cavities. In both cases, the resolution of the grid was 60×60×60 points with a grid spacing of 0.450 Å. Each substrate was docked into the grid with the Lamarckian algorithm as implemented in AutoDock. The ligand bonds were allowed to freely rotate during docking The genetic-based algorithm ran 20 simulations per substrate with 2,000,000 energy evaluations and a maximum number of generations of 27,000. The crossover rate was increased to 0.8, and the number of individuals in each population to 150. All other parameters were left at the AutoDock default settings.

Neuroprotection Assays

Primary cortical neuron cultures were obtained from the cerebral cortex of fetal Sprague-Dawley rats (embryonic day 17) as described previously. All experiments were initiated 24 h after plating. Under these conditions, the cells are not susceptible to glutamate-mediated excitotoxicity. For cytotoxicity studies, cells were rinsed with warm PBS and then placed in minimum essential medium (Invitrogen) containing 5.5 g/liter glucose, 10% fetal calf serum, 2 mM L-glutamine, and 100 μM cystine. Oxidative stress was induced by the addition of the

glutamate analog homocysteate (HCA; 5 mM) to the media. HCA was diluted from 100-fold concentrated solutions that were adjusted to pH 7.5. In combination with HCA, neurons were treated with either TSA or Tubastatin A at the indicated concentrations. Viability was assessed after 24 h by MTT assay (3-(4,5-dimethylthiazol-2-yl)- 2,5-diphenyltetrazolium bromide) method.

Supplementary Material

Refer to Web version on PubMed Central for supplementary material.

Acknowledgments

This work was supported by the National Institutes of Health [R01 AG022941] (A. K.). K. B. is supported by an American Chemical Society division of medicinal chemistry predoctoral fellowship. We also thank the International Rett Syndrome Foundation for their support allowing the scale up and ADMET studies on Tubastatin A.

References

1. Xu WS, Parmigiani RB, Marks PA. Oncogene. 2007; 26:5541–5552. [PubMed: 17694093]
2. Choudhary C, Kumar C, Gnad F, Nielsen ML, Rehman M, Walther TC, Olsen JV, Mann M. Science. 2009; 325:834–840. [PubMed: 19608861]
3. Kelly WK, Marks PA. Nat. Clin. Pract. Oncol. 2005; 2:150–157. [PubMed: 16264908]
4. Dokmanovic M, Clarke C, Marks PA. Mol. Cancer Res. 2007; 5:981–989. [PubMed: 17951399]
5. de Ruijter AJ, van Gennip AH, Caron HN, Kemp S, van Kuilenburg AB. Biochem. J. 2003; 370:737–749. [PubMed: 12429021]
6. Glaser KB, Li J, Staver MJ, Wei RQ, Albert DH, Davidsen SK. Biochemical and biophysical research communications. 2003; 310:529–536. [PubMed: 14521942]
7. Witt O, Deubzer HE, Milde T, Oehme I. Cancer Lett. 2009; 277:8–21. [PubMed: 18824292]
8. Drummond DC, Noble CO, Kirpotin DB, Guo Z, Scott GK, Benz CC. Annu. Rev. Pharmacol. Toxicol. 2005; 45:495–528. [PubMed: 15822187]
9. Minucci S, Pelicci PG. Nat. Rev. Cancer. 2006; 6:38–51. [PubMed: 16397526]
10. Thomas EA. Mol. Neurobiol. 2009; 40:33–45. [PubMed: 19396637]
11. Grozinger CM, Hassig CA, Schreiber SL. Proc. Natl. Acad. Sci. U S A. 1999; 96:4868–4873. [PubMed: 10220385]
12. Boyault C, Sadoul K, Pabion M, Khochbin S. Oncogene. 2007; 26:5468–5476. [PubMed: 17694087]
13. Hubbert C, Guardiola A, Shao R, Kawaguchi Y, Ito A, Nixon A, Yoshida M, Wang XF, Yao TP. Nature. 2002; 417:455–458. [PubMed: 12024216]
14. Kovacs JJ, Murphy PJ, Gaillard S, Zhao X, Wu JT, Nicchitta CV, Yoshida M, Toft DO, Pratt WB, Yao TP. Mol. Cell. 2005; 18:601–607. [PubMed: 15916966]
15. Wang Z, Zang C, Cui K, Schones DE, Barski A, Peng W, Zhao K. Cell. 2009; 138:1019–1031. [PubMed: 19698979]
16. Wang L, de Zoeten EF, Greene MI, Hancock WW. Nat. Rev. Drug Discov. 2009; 8:969–981. [PubMed: 19855427]
17. Dompierre JP, Godin JD, Charrin BC, Cordelieres FP, King SJ, Humbert S, Saudou F. J. Neurosci. 2007; 27:3571–3583. [PubMed: 17392473]
18. Kazantsev AG, Thompson LM. Nat. Rev. Drug Discov. 2008; 7:854–868. [PubMed: 18827828]
19. Rivieccio MA, Brochier C, Willis DE, Walker BA, D'Annibale MA, McLaughlin K, Siddiq A, Kozikowski AP, Jaffrey SR, Twiss JL, Ratan RR, Langley B. Proc. Natl. Acad. Sci. U S A. 2009; 106:19599–19604. [PubMed: 19884510]
20. Wong JC, Hong R, Schreiber SL. J. Am. Chem. Soc. 2003; 125:5586–5587. [PubMed: 12733869]

21. Haggarty SJ, Koeller KM, Wong JC, Grozinger CM, Schreiber SL. Proc. Natl. Acad. Sci. U S A. 2003; 100:4389–4394. [PubMed: 12677000]
22. Schafer S, Saunders L, Schlimme S, Valkov V, Wagner JM, Kratz F, Sippl W, Verdin E, Jung M. ChemMedChem. 2009; 4:283–290. [PubMed: 19090524]
23. Itoh Y, Suzuki T, Kouketsu A, Suzuki N, Maeda S, Yoshida M, Nakagawa H, Miyata N. J. Med. Chem. 2007; 50:5425–5438. [PubMed: 17929798]
24. Manku S, Allan M, Nguyen N, Ajamian A, Rodrigue J, Therrien E, Wang J, Guo T, Rahil J, Petschner AJ, Nicolescu A, Lefebvre S, Li Z, Fournel M, Besterman JM, Deziel R, Wahhab A. Bioorg. Med. Chem. Lett. 2009; 19:1866–1870. [PubMed: 19272776]
25. Roy A, Kucukural A, Zhang Y. Nat. Protoc. 5:725–738. [PubMed: 20360767]
26. Kozikowski AP, Tapadar S, Luchini DN, Kim KH, Billadeau DD. J. Med. Chem. 2008; 51:4370–4373. [PubMed: 18642892]
27. Somoza JR, Skene RJ, Katz BA, Mol C, Ho JD, Jennings AJ, Luong C, Arvai A, Buggy JJ, Chi E, Tang J, Sang BC, Verner E, Wynands R, Leahy EM, Dougan DR, Snell G, Navre M, Knuth MW, Swanson RV, McRee DE, Tari LW. Structure. 2004; 12:1325–1334. [PubMed: 15242608]
28. Kozikowski AP, Chen Y, Gaysin A, Chen B, D'Annibale MA, Suto CM, Langley BC. J. Med. Chem. 2007; 50:3054–3061. [PubMed: 17539623]
29. Parmigiani RB, Xu WS, Venta-Perez G, Erdjument-Bromage H, Yaneva M, Tempst P, Marks PA. Proc. Natl. Acad. Sci. U S A. 2008; 105:9633–9638. [PubMed: 18606987]

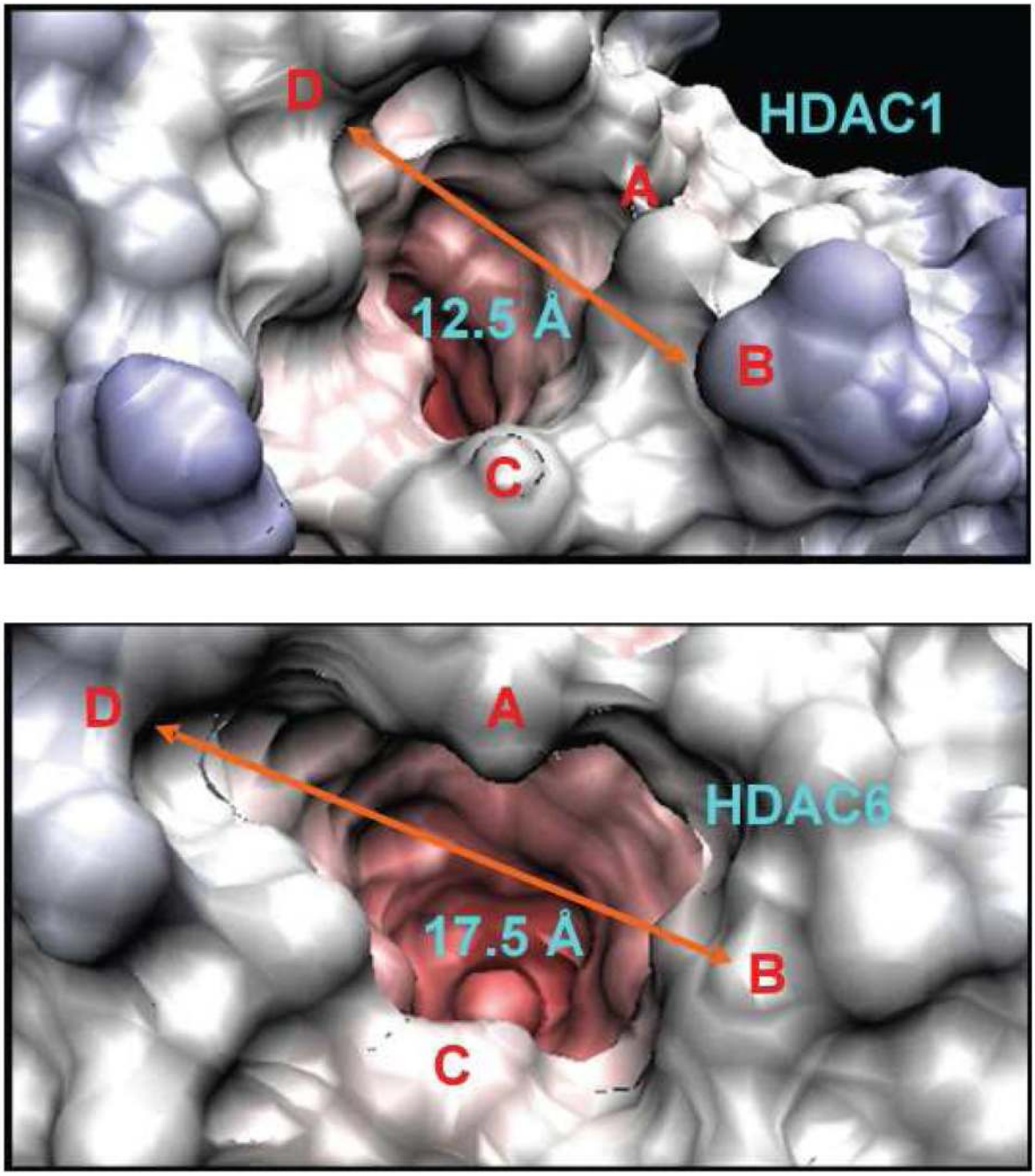

Figure 1.
Top-down view of active site for homology models of HDAC1 (top) and HDAC6 (bottom). Distances between boundaries of the catalytic channel rim are shown with orange arrows. Letters A–D denote four boundary areas surrounding the channel rim.

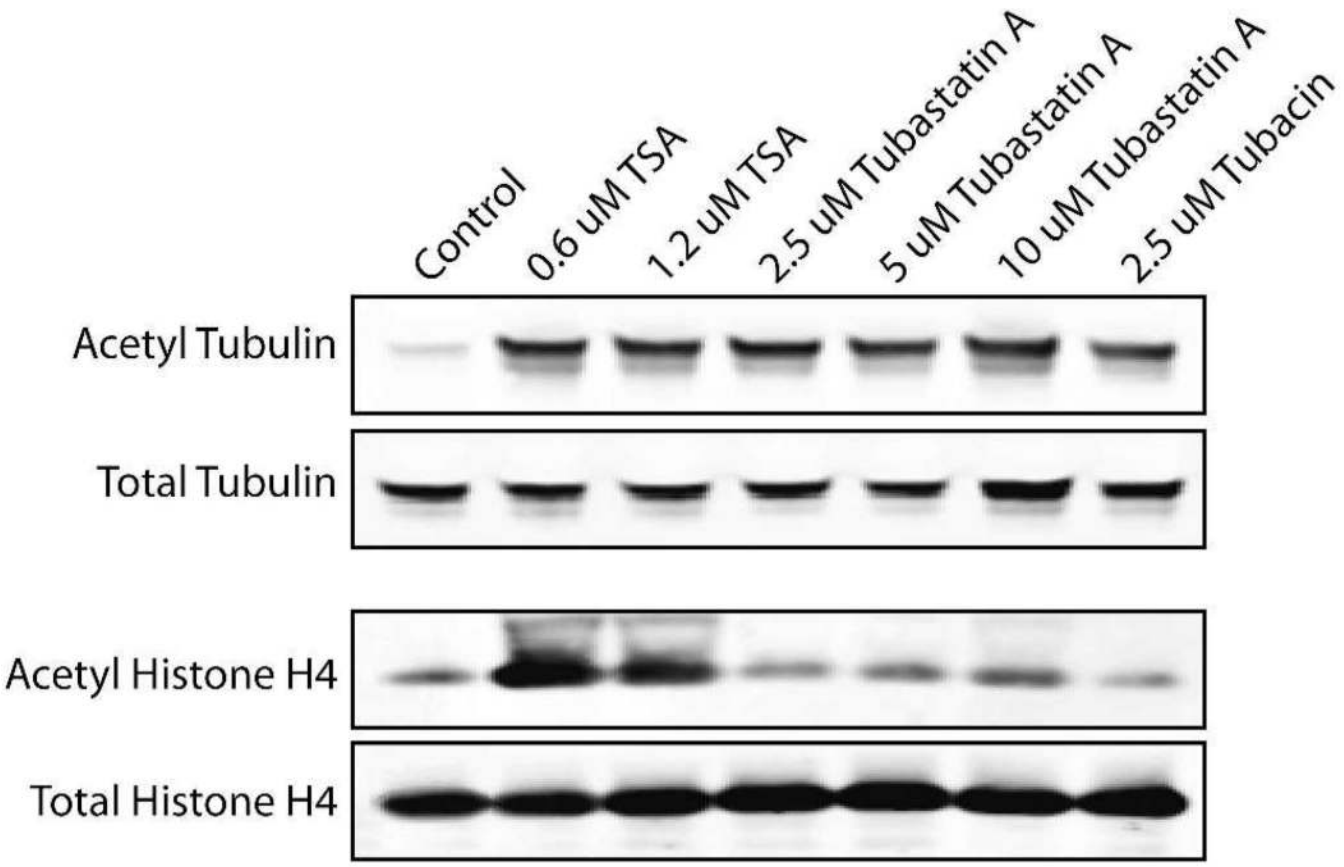

Figure 2.
Comparison of histone and α-tubulin hyperacetylation for TSA, Tubastatin A, and Tubacin.

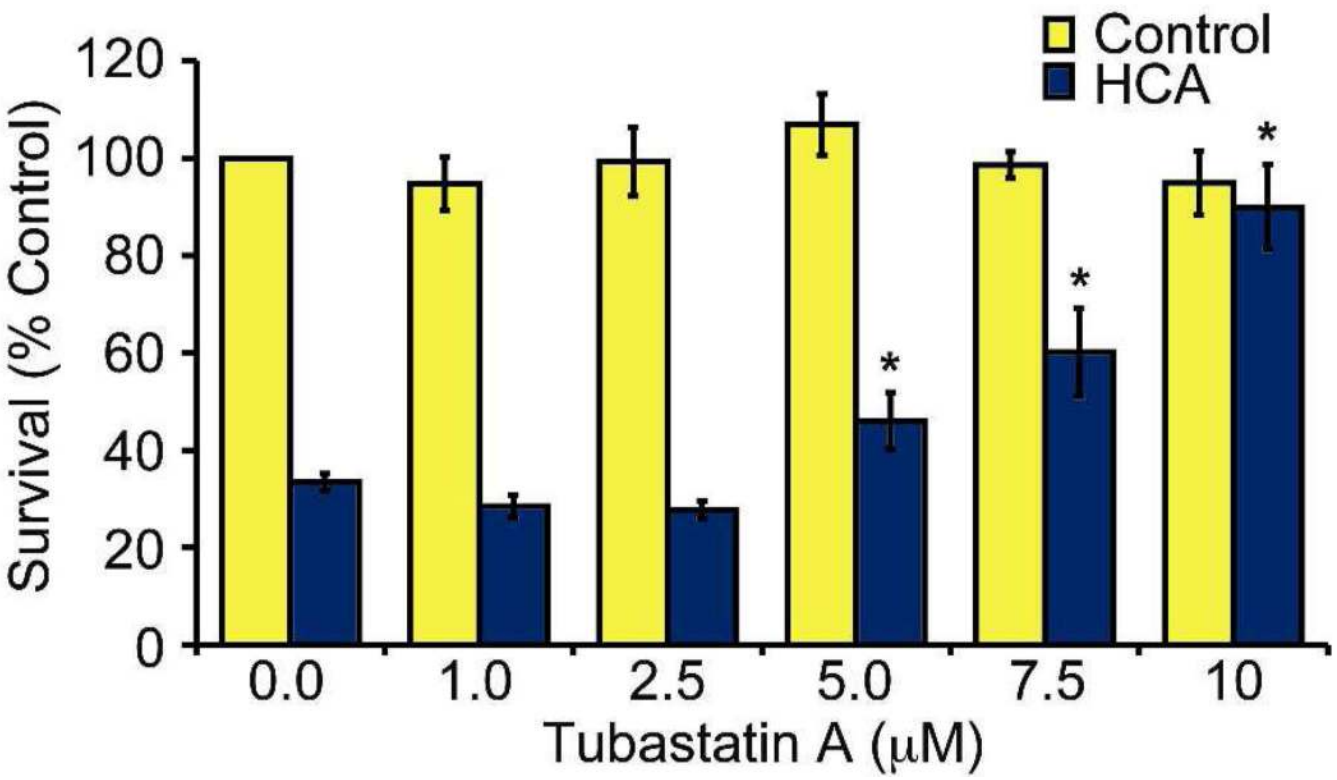

Figure 3.

HCA oxidative stress assay: neurons were treated with Tubastatin A, with or without addition of HCA. Viability was assessed after 24 h by MTT assay. Yellow bars: Tubastatin A alone; Blue bars: Tubastatin A + HCA. *, significant increase in survival relative to HCA-treated control, $P < 0.01$, by two-way ANOVA followed by Bonferroni post-tests.

Table 1

HDAC inhibition data for **1–7** and other referenced inhibitors.

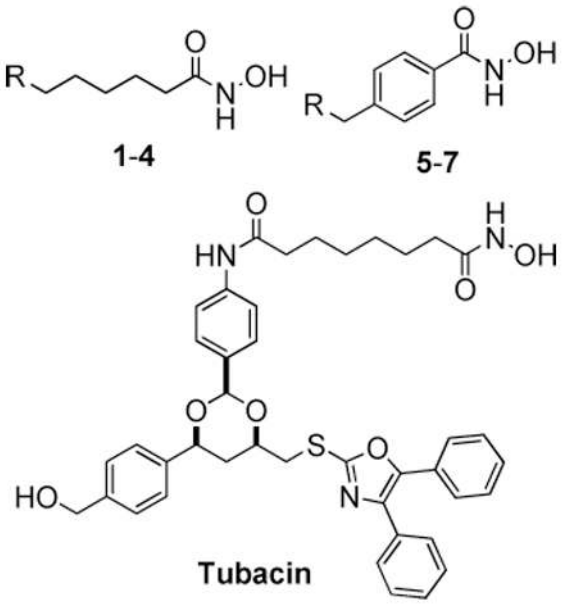

	R=	HDAC1 IC_{50} (μM) ± SD	HDAC6 IC_{50} (μM) ± SD
1	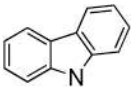	14.0 ± 4.8	0.062 ± 0.004
2	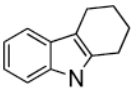	8.6 ± 3.7	0.090 ± 0.019
3	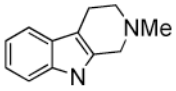	>30	0.550 ± 0.002
4	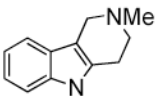	25.2 ± 3.3	0.213 ± 0.044
5	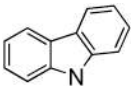	10.9 ± 3.4	0.019 ± 0.001
6 (Tubastatin A)	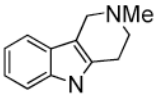	16.4 ± 2.6	0.015 ± 0.001
7	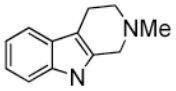	5.18 ± 0.12	0.0014 ± 0.0003
TSA	N/A	4.74 ± 1.26	1.21 ± 0.49
Tubacin	N/A	1.40 ± 0.24	0.004 ± 0.001

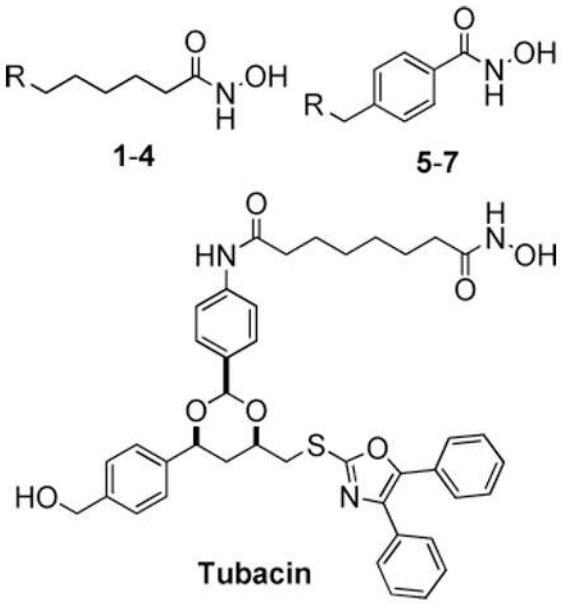

	R=	HDAC1 IC_{50} (μM) ± SD	HDAC6 IC_{50} (μM) ± SD
ISOX[a]	N/A	0.071 ± 0.059	0.0024 ± 0.0021

Data are shown as IC_{50} values in μM ±standard deviation. Values are the mean of two experiments, except TSA, which is a mean of 9 experiments. Compounds were tested in duplicate in a 10-dose IC_{50} mode with 3-fold serial dilution starting from 30 μM solutions. IC_{50} values were extracted by curve-fitting the dose/response slopes. TSA was used as an internal standard.

[a]This isoxazole-based inhibitor (**ISOX**) was previously reported by our group to have a low picomolar IC_{50} at HDAC6.26 When this compound was tested in the present assays, a more reasonable value was observed. After investigating the source of this discrepancy, we found that lack of a detergent (Triton ×100) in the original assay caused the anomalously high activity. Screening was performed by Reaction Biology (Malvern, PA).

Table 2

Enzyme inhibition data for Tubacin and Tubastatin A at all 11 HDAC isozymes.

	Tubacin	Tubastatin A
	IC_{50} (μM) ± SD	**IC_{50} (μM) ± SD**
HDAC1	1.40 ± 0.24	16.4 ± 2.6
HDAC2	6.27 ± 0.29	>30
HDAC3	1.27 ± 0.16	>30
HDAC4	17.3 ± 2.1	>30
HDAC5	3.35 ± 0.03	>30
HDAC6	0.004 ± 0.001	0.015 ± 0.001
HDAC7	9.7 ± 1.8	>30
HDAC8	1.27 ± 0.16	0.854 ± 0.040
HDAC9	4.31 ± 0.34	>30
HDAC10	3.71 ± 0.16	>30
HDAC11	3.79 ± 0.10	>30

Values are the mean of two experiments. Data are shown as IC_{50} values in μM ± standard deviation. Compounds were tested in duplicate in 10-dose IC_{50} mode with 3-fold serial dilution starting from 30 μM solutions. IC_{50} values were extracted by curve-fitting the dose/response slopes.